Journal of Structural Geology, Vol. 11, No. 6, pp. 669 to 678, 1989
Printed in Great Britain

0191-8141/89 $03.00 + 0.00

Measuring displacement gradients and strains in faulted rocks

STEVEN WOJTAL

Department of Geology, Oberlin College, Oberlin, OH 44074, U.S.A.

(*Received* 6 *June* 1988; *accepted in revised form* 27 *February* 1989)

Abstract—In homogeneous deformations, spatial gradients of the displacement field are constant and related to strain parameters by straightforward algebraic relationships. Deformations which are inhomogeneous (displacement gradients values are not constant) when viewed at one scale may be statistically homogeneous (have approximately constant displacement gradients) when viewed at a smaller scale. From average values of the displacement gradients in a statistically homogeneous deformation, one can calculate bulk strains. *Displacement diagrams* provide a way to determine the displacements of material points at different positions within inhomogeneously deformed media. From these data, one may measure mean values of the displacement gradients for the deformation, and if the gradients are approximately constant, calculate bulk strains. This strain measurement technique yields reasonable strain values. Strain values from a natural fault array in the Tennessee Appalachians (U.S.A.) differ slightly from values reported earlier, but still conform with kinematic indicators in those deformed rocks.

INTRODUCTION

IN CONTINUOUS deformations, displacement vectors vary smoothly with position, displacement gradients are finite and strain values exist at all points. Continuous deformations may be homogeneous, where displacement gradients and strain values are independent of position, or inhomogeneous, where displacement gradients and strain values vary with position (Ramsay 1967, 1969). In discontinuous deformations, displacement vectors do not vary smoothly with position, displacement gradients are not finite at all points, and strain values do not exist where displacement gradients are undefined. Whether we perceive a particular displacement vector field to be continuous or discontinuous, however, depends on the scale at which we observe the deformation (King 1983). Deformations which appear discontinuous at one scale may appear continuous if the observation scale is magnified or reduced sufficiently (Ramsay 1969). The kinematic character noted for a particular deformation at a given observation scale should not be construed as indicating in any way the mechanical processes by which the deformation accrued. When observed at the appropriate scale, crystal–plastic deformation mechanisms generate discontinuous displacement vector fields (e.g. fig. 2.5 in Ramsay & Huber 1983). Brittle processes may generate macroscopically ductile deformations with apparently continuous displacement vector fields (see discussion in Rutter 1986).

Consider deformations which are inhomogeneous at the scale of a hand sample or an outcrop, with localized regions like ductile deformation zones (DDZs) where strains are relatively high within a medium where strains are relatively low. If this locally inhomogeneous deformation is statistically homogeneous (Paterson & Weiss 1961), it is meaningful to define bulk strain values for the deformation. Cobbold (1977) used strain values within and between the high strain regions to fix the components of a deformation gradient tensor and thereby calculate bulk strain values in continuous but inhomogeneous deformations. In principle his method applies to rocks cut by any one of many kinematically equivalent deformation elements such as DDZs, kink bands or deformation bands. Minor faults are kinematically equivalent to DDZs, and kinematic patterns in minor fault arrays may suggest that the bulk deformation due to fault movement is statistically homogeneous (Price 1967, Arthaud 1969, Wojtal 1982, 1986). The difficulty of defining strains *within* fault zones, however, renders Cobbold's method impractical in faulted rocks. Bulk strains due to movement on faults in arrays can be measured by other methods only in special circumstances (Jamison & Higgs 1987, Kranz 1988), so most structural studies of faulted rocks, even when offsets on faults are known, focus on fault kinematics (Arthaud 1969, Arthaud & Mattauer 1969, Arthaud & Choukroune 1972, Etchecopar *et al.* 1981, Angelier 1984, Hancock 1985). Studies of fault kinematics are often augmented by estimating longitudinal strains in key beds (Cooper *et al.* 1983) or rocks adjacent to faults (Williams & Chapman 1983).

One can calculate meaningful bulk strain values for statistically homogeneous deformations when average values of spatial gradients of the displacement field are known. A geometrical construction here called a *displacement diagram*, which gives insight to how fault displacements change where faults curve or join (Wojtal 1982, McCaig 1988), can be used to measure mean displacement gradients in faulted or pressure-solved rocks. Displacement diagrams provide, therefore, a way to convert measurements of displacements on faults or across stylolites into bulk strain values for some discontinuous deformations. This technique may contribute to studies of faulted rocks by helping to include strain data in balanced cross-sections of low-grade terranes (Woodward *et al.* 1986) and to understand the

bulk material properties of faulted rocks (Wojtal 1982, 1986, Wojtal & Mitra 1986).

STRAIN VALUES AND DISPLACEMENT GRADIENTS IN CONTINUOUS DEFORMATIONS

Transformation equations which relate the positions of material points in the undeformed state to the positions of corresponding points in the deformed state are the basis of all strain measurements (Ramsay 1976, Ramsay & Huber 1983, pp. 55–71). I here choose the final state as reference state, and use the *Eulerian* specification of the transformation equations (Ramsay 1976, Ramsay & Huber 1983, p. 20)

$$\mathbf{x} = f(\mathbf{x}'), \tag{1}$$

where $\mathbf{x}$ is the position vector of a material point in the undeformed state and $\mathbf{x}'$ is the position vector of the corresponding material point in the deformed state measured relative to the same origin. In all that follows, unprimed quantities refer to the undeformed state, and primed quantities refer to the deformed state. The vector difference between positions in the undeformed and deformed states

$$\mathbf{u}'(\mathbf{x}') = \mathbf{x} - \mathbf{x}' = f(\mathbf{x}') - \mathbf{x}' \tag{2}$$

is the reciprocal displacement of the point $\mathbf{x}'$. Both f and $\mathbf{u}'$ are continuous functions of $\mathbf{x}'$ in continuous deformations.

Spatial derivatives of the reciprocal displacement vector field are

$$\partial u_i'/\partial x_j' = \mathbf{E}_{ij} - \delta_{ij}, \tag{3a}$$

where $\mathbf{E}_{ij} = \partial f_i/\partial x_j'$ and δ_{ij} is the Kronecker delta ($\delta_{ij} = 1$ when $i = j$ and $\delta_{ij} = 0$ when $i \neq j$). After rearranging and in matrix form, equations (3a) are

$$\mathbf{E} = \partial \mathbf{u}'/\partial \mathbf{x}' + \mathbf{I}, \tag{3b}$$

where $\mathbf{E}$ is the reciprocal deformation matrix and $\mathbf{I}$ is the identity matrix.

Familiar strain parameters, like the reciprocal quadratic elongation, λ' (Ramsay & Huber 1983, p. 281), are algebraic functions of displacement gradients values. Cutler & Elliott (1983) showed that

$$\boldsymbol{\lambda}' = \mathbf{E}^{\mathrm{T}}\mathbf{E}, \tag{4}$$

where $\mathbf{E}^{\mathrm{T}}$ is the transpose of $\mathbf{E}$. Substituting from equation (3b),

$$\boldsymbol{\lambda}' = [\mathbf{I} + \partial \mathbf{u}'/\partial \mathbf{x}']^{\mathrm{T}}[\mathbf{I} + \partial \mathbf{u}'/\partial \mathbf{x}']. \tag{5}$$

Equation (5) holds at all points in a continuously deformed body where the reciprocal displacement vector field is known.

In geology, it is common to derive finite strain values from measured changes in the shapes of ellipsoidal or spherical objects or measured changes in the lengths of and/or angles between material lines. For the reciprocal quadratic elongation, longitudinal strains in the x_i' co-ordinate direction are

$$\lambda_{ii}' = (l/l')^2, \tag{6a}$$

where l' is the length of a material line parallel to the x_i' direction in the deformed state and l was the original length of that material line. Shear strains in the x_j' co-ordinate direction on a plane whose normal is the x_i' co-ordinate direction are

$$\lambda_{ij}' = \lambda_{ii}'(\tan \psi_{ij}), \tag{6b}$$

where ψ_{ij} is the angular shear of a line in the x_j' direction.

In homogeneous finite deformations: (1) material lines which were straight in the undeformed state are straight in the deformed state; (2) material lines which were parallel in the undeformed state are parallel in the deformed state; and (3) the ratios of lengths of corresponding segments of a single material line in the undeformed and deformed states are unchanged by deformation (Ramsay 1976). Ellipsoidal and spherical objects in the undeformed state are transformed into other ellipsoids by homogeneous deformations.

Since the strain values λ_{ij}' in equation (5) are defined at individual points, their relationship to measured changes of lengths or angles in a real deformation is approximate. In order for the straight line/parallel line criteria to hold, λ' values must be essentially constant across the region of interest. In homogeneous deformations, then, the reciprocal displacement vector field is not only continuous, but its derivatives, $\partial \mathbf{u}'/\partial \mathbf{x}'$, are continuous and constant-valued (Elliott 1970, Ramsay & Huber 1983, p. 15). In a homogeneous deformation, equations (1)–(3) become

$$\mathbf{x} = \mathbf{E} \cdot \mathbf{x}' \tag{1a}$$

$$\mathbf{u}' = (\mathbf{E} - \mathbf{I}) \cdot \mathbf{x}' \tag{2a}$$

$$\partial \mathbf{u}'/\partial \mathbf{x}' = \mathbf{E} - \mathbf{I}, \tag{3a}$$

where $\mathbf{E}$ is a matrix whose elements are constant valued.

Gradients of reciprocal displacement vector fields are never constant in nature. It is customary to treat real, that is inhomogeneous, deformations by dividing them into numerous small regions where, when viewed at a larger scale, gradients of the reciprocal displacement vector field are essentially constant and deformation is homogeneous (Ramsay 1976). It is equally plausible to reduce our observation scale and search for broader scale homogeneity in the reciprocal displacement vector field. By explicitly stating the criterion for homogeneity in terms of displacement gradients, we have an arbitrary way to judge whether a deformation is statistically homogeneous: deformation is statistically homogeneous at a scale where displacement vector field gradients in the rocks are approximately constant. If the values of the displacement vector field gradients can be measured, we can calculate bulk strains with equation (5) or its equivalent.

DISPLACEMENT GRADIENTS AND STRAIN VALUES IN DISCONTINUOUS DEFORMATIONS

When kinematic analysis suggests that faults, veins or stylolites are elements in a deformation which is statis-

tically homogeneous at a scale larger than the individual elements (Price 1967, Arthaud 1969, Wojtal 1986), one may test for statistical homogeneity by measuring gradients of the displacement vector field. I illustrate below how displacement diagrams can be used to convert standard field data, measured offsets on faults or across veins or stylolites, to reciprocal displacement vector field gradient values.

The idea underlying the displacement diagram is to depict, in an organized manner, the reciprocal displacement vectors of the material points in a limited region relative to an origin located within that region. Inasmuch as the displacement diagram summarizes the displacements of material points at different positions in a deformed body, it is just a bookkeeping method for field data. The *hodograph*, or velocity plane construction, used in plane plastic flow (Ford 1963, pp. 491–499) is the inspiration for this use of displacement diagrams, but the diagrams are used, in practice, like the velocity plane constructions used to analyze plate motions (McKenzie & Parker 1967, Cox & Hart 1986, pp. 51–83) or the stability of intersecting faults (McCaig 1988). Like velocity plane diagrams or Mohr diagrams, displacement diagrams are images in a separate graphical space (e.g. velocity space or Mohr space) of a deformation which occurs in 'physical' space. In the case of the displacement diagram, we draw a graphical image in displacement space. It is, in principle, possible to construct three-dimensional displacement diagrams using stereovectors on an orthographic net (De Paor 1979, 1983). I will, however, here consider only planar principal sections through homogeneous deformations where displacements are confined to the section plane or displacements normal to the section plane are equal, i.e. (1) area ratios are constant in the section plane and (2) nearby principal planes parallel the section plane (Cutler & Elliott 1983).

To draw this type of displacement diagram, choose a material point (O′) as an origin, and measure local reciprocal displacement vectors for other material points P′, Q′, etc., relative to O′ (Fig. 1a). If material point O′ were displaced during deformation, one would add a bulk translation vector to local reciprocal displacement vectors to determine the total reciprocal displacements of material points near O′. Each material point in the vicinity of O′ has an image point on the displacement plane. Plot o′, the displacement plane image of O′, at the origin of the displacement diagram. Plot p′, the image of P′, so that the vector o′p′ parallels the reciprocal displacement vector for material point P′ relative to the origin O′ and the length of o′p′ is proportional to the magnitude of the reciprocal displacement vector for point P′ relative to the origin O′ (Fig. 1b). Rays emanating from the origin o′ to distinct image points p′ or q′ give the reciprocal displacement vectors of material points P′ or Q′ relative to the origin O′. Chords connecting distinct image points p′ and q′ give the reciprocal displacement vectors of one material point (P′) relative to another material point (Q′). If two material points have the same reciprocal displacement vector relative to the origin (e.g. both lie in a rock mass which suffered solid body translation), they have a single displacement plane image point (the chord connecting them has zero length).

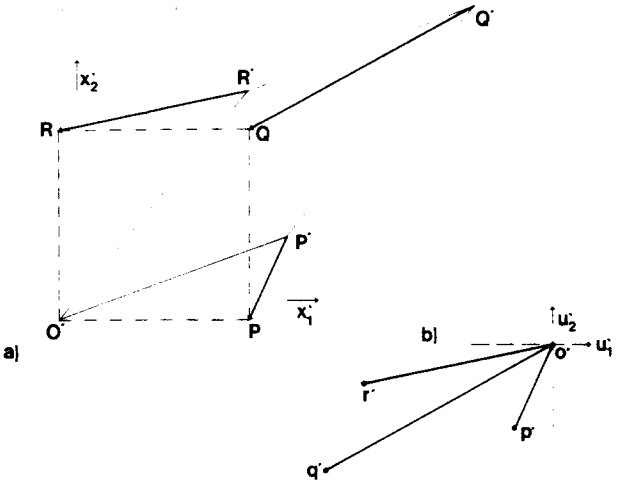

Fig. 1. (a) Homogeneous deformation transforms a square (dashed lines) into a parallelogram (solid lines), displacing point P to P′, point Q to Q′ and point R to R′. (b) Diagram giving displacement plane images of corners in homogeneous deformation in (a). See text for explanation.

Faulted rocks

Figure 2(a) shows a hypothetical rock mass cut by an array of planar faults where fault-bounded blocks are translated parallel to fault planes. Material points within each fault-bounded block have equal reciprocal displacement vectors relative to the origin and plot at a single image point. Point o′ in Fig. 2(b) is the displacement plane image of all material points in block O′, here assumed to be stationary. Block A moved relative to block O along fault ff_1; the reciprocal displacement vector for block A′ is f′f. Point a′, the displacement plane image of block A′, plots so that o′a′ is parallel and proportional to f′f. Displacement plane images of blocks

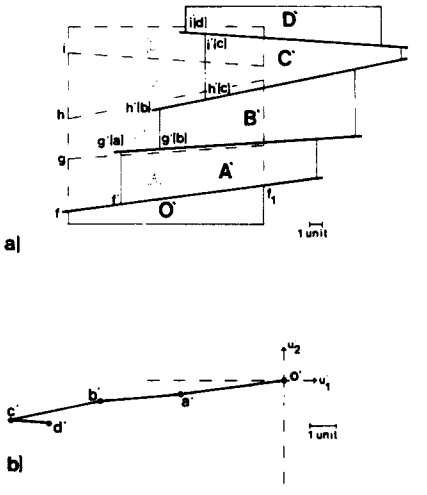

Fig. 2. (a) A hypothetical fault array transforms a square (dashed lines) into a collection of rigid blocks which have been translated relative to their neighbours. (b) Diagram giving displacement plane images of selected material points in this discontinuous deformation. See text for explanation.

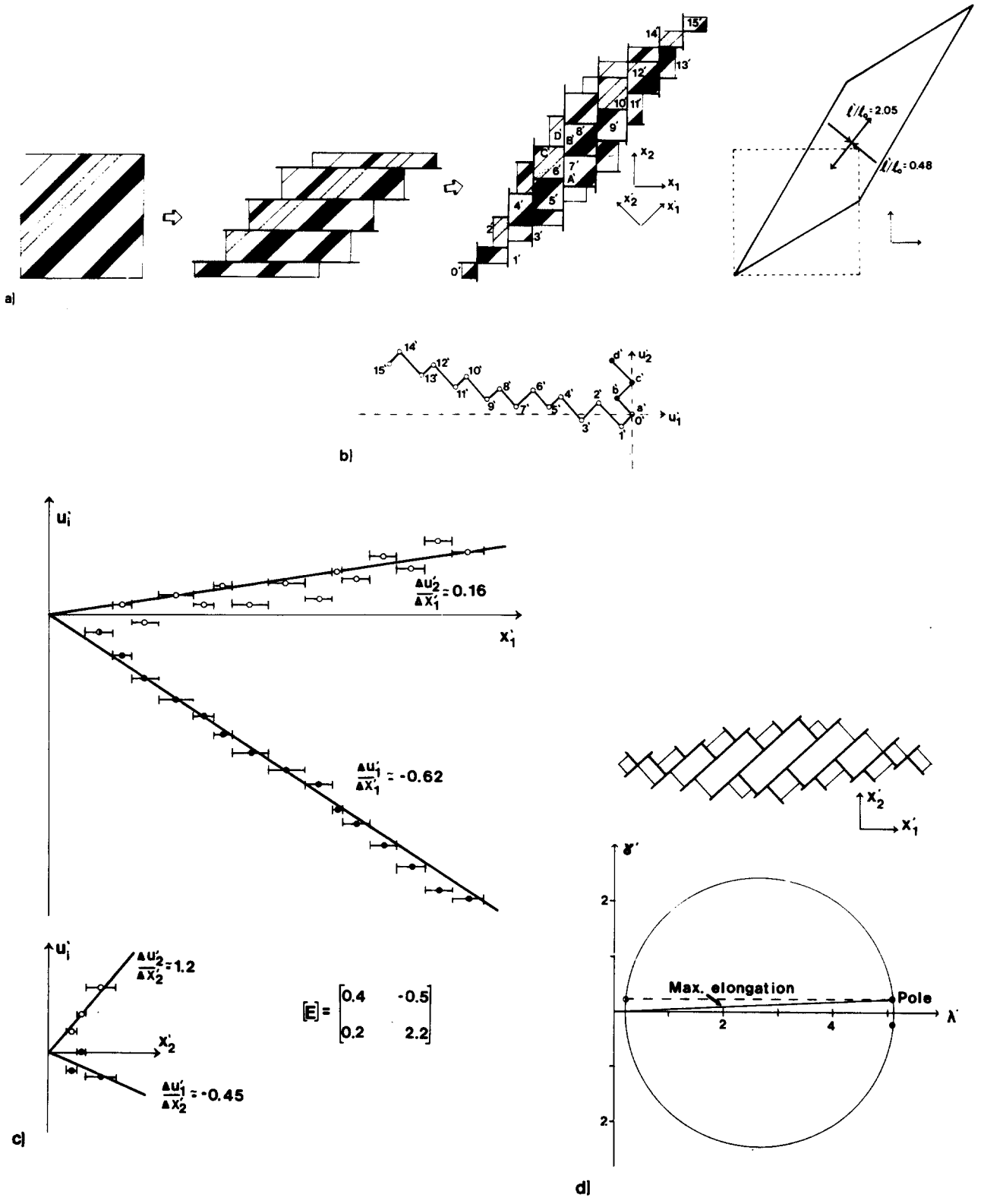

Fig. 3. (a) Deformation of a rock mass by two hypothetical fault arrays. Imposed offsets on faults produce net displacements of material points which correspond to those in the homogeneous deformation illustrated at right. (b) Diagram showing displacement-plane images of fault-bounded blocks crossed by traverses along the x'_1–x'_2 axes in (a). (c) Plots of components of the cumulative displacement (relative to the origin at the end of each traverse) of fault-bounded blocks (u'_i) vs distance along the traverse (x'_j). Closed circles give u'_1 components, and open circles give u'_2 components. The 'error bars' give the length of each fault-bounded block crossed during the traverse. The heights of the 'steps' from point to point give the components of the reciprocal displacement on faults between blocks. $\Delta u'_i/\Delta x'_j$ values are estimated from 'eyeball' fits to data. Components of the reciprocal deformation matrix **E** calculated using equations (3). The calculated area ratio = 1/(det **E**) = 1.02. (d) Mohr diagram for reciprocal quadratic elongation, drawn using λ' values calculated from displacement gradient values in (c); the physical plane sketch above the Mohr diagram shows attitudes of the x'_1–x'_2 axes for plotted position of the pole to the Mohr circle. The measured orientations of the principal directions differ from the principal directions of the imposed deformation by 1°. The measured maximum stretch value is 2.23; the maximum stretch of the imposed deformation is 2.05. The measured minimum stretch value is 0.44; the minimum stretch of the imposed deformation is 0.48.

B′, C′ and D′, plotted in the same manner, are b′, c′ and d′, respectively. Note that o′c′, the reciprocal displacement of block C′ relative to the origin, is the resultant of the reciprocal displacement vectors of block C′ relative to block B′, block B′ relative to block A′ and block A′ relative to the origin.

Because the displacement diagram uses only the net displacement of material points, we require no information on the relative ages of the faults. In Fig. 3, the net displacements of blocks not contiguous with the origin (blocks 2′–15′) are products of displacements on segments of individual faults which were active at different times. Each distinct traverse from the origin to a particular fault-bounded block must yield the same net displacement. Thus, different traverses from the origin to each block generate different sets of rays and chords whose resultants must be the same.

In strained rocks, net displacements of material points change with position. A displacement diagram constructed from the attitudes, offsets and spacings of faults encountered along a straight line traverse across a fault array will give the net displacements of fault-bounded blocks along that traverse. Plots of the displacement components of material points which lie along a straight line traverse vs the distance between the material points show how displacements change with position. If deformation is statistically homogeneous, first-order terms account for most of the change in displacement with position and plotted points define a straight line. If deformation is not statistically homogeneous, a plot of displacement component values vs distance will not define a straight line. If deformation is statistically homogeneous, measuring the slopes of displacement vs distance plots for two orthogonal traverses across a section provides a way to estimate values of displacement gradients in the faulted rocks, and thereby to calculate bulk strain values for deformation due to faulting.

In Fig. 3(a), the net displacements of material points due to movement on faults conform with an arbitrary homogeneous deformation. The x_1'–x_2' axes in Fig. 3(a) are orthogonal traverse lines, with arbitrary orientations across the section, which define right-handed, Cartesian co-ordinates. Figure 3(b) gives the reciprocal displacements, relative to an 'origin' at one end of each traverse, of fault-bounded blocks encountered along each traverse. The net reciprocal displacements of blocks 1′, 2′, 3′, etc., along a traverse are the resultants 0′1′, 0′2′, 0′3′, etc., on the displacement diagram. The present distance between blocks and the origin can be measured directly on Fig. 3(a). Figure 3(c) is a plot of the reciprocal displacement vector components (u_i') vs distance along the traverse. Since deformation is statistically homogeneous, u_i' vary linearly with x_j', and the plots of u_i' vs x_j' approximate straight lines. The slopes of these lines, $\Delta u_i'/\Delta x_j'$, are average values of the displacement gradients $\partial u_i'/\partial x_j'$. A Mohr diagram for reciprocal quadratic elongations (Fig. 3d), calculated using equation (5), gives strain principal values, strain principal directions and area ratios for the bulk deformation; they are good estimates of the imposed strains. Wojtal (1982, 1986) used the slopes and intercepts of two plots of u_i' vs x_1' to estimate the four displacement gradient values, but four u_i' vs x_j' plots yield more reliable estimates of the imposed displacement gradients in test cases.

This technique, which relies upon an averaging of displacements at different distances from arbitrary origins in a rock, may yield bulk strain values which, while they are in good agreement with physical features developed in the rock, are misleading inasmuch as the deformation is not homogeneous in a strict sense. In fact, it is always possible to use the net displacements of material points at some distance from the origin to define 'average' values of displacement gradients (Fig. 4). Whether these 'average' values are good estimates of the displacement gradients throughout an area depends upon the nature of the deformation (Fig. 4). The proposed method requires, like all strain measurement methods, judgement to be used most effectively.

If faults have bends or are curved, and no gaps or overlaps form during deformation, fault-bounded blocks cannot remain rigid. In the simple case illustrated in Fig. 5(a), a fault-bend fold (Suppe 1983) formed in the fault's hangingwall. Since different portions of the hangingwall

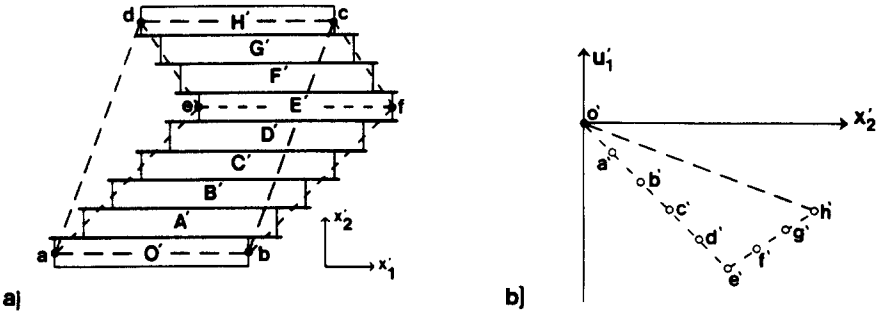

Fig. 4. (a) A section through a hypothetical deformation where slip on discrete surfaces produced bulk inhomogeneous simple shear. The total deformation comprises two regions of homogeneous simple shear. Note the orientations of the x_1'–x_2' axes. (b) A plot of displacement component u_1' vs distance x_2' across the section. Parallelogram abcd connotes the shape change estimated from the net offset of block H′ relative to block O′, i.e. where the slope of the line o′h′ estimates $\partial u_1'/\partial x_2'$ in the deformation. The displacement vs distance plot, however, is composed of straight line segments o′e′ and e′h′, each corresponding to a region of uniform simple shear. The true shape change is connoted by the two parallelograms abfe and cdef.

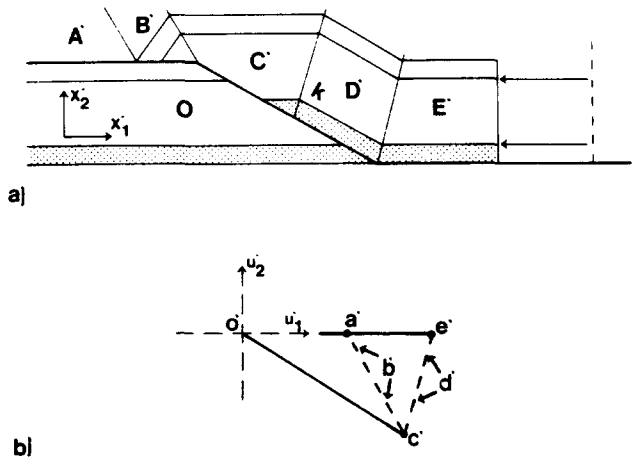

Fig. 5. (a) A fault hangingwall must deform as it moves over a rigid footwall on a curved fault. (b) Displacement plane images of selected points in (a). The displacement plane image of different portions of the hangingwall (a', c' and e') move farther from the origin o' as net displacement on the fault increases. If ramp height is fixed, their resultant displacement vectors (o'a', o'c' and o'e') become more nearly equal.

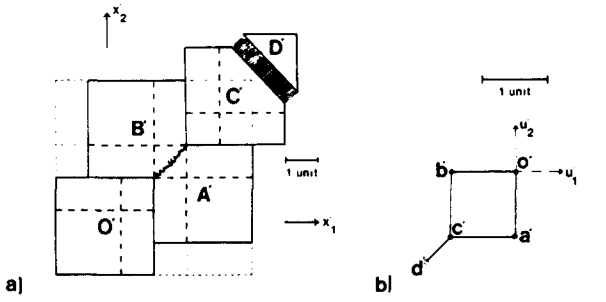

Fig. 7. (a) Hypothetical deformation where rigid blocks move relative to each other by removing material from some boundaries and adding it along others. (b) Diagram giving displacement-plane images of selected material points in the deformation portrayed in (a). The series of chords between displacement plane images of fault-bounded blocks encountered during a closed-loop traverse in physical space form a closed-loop if displacements on block boundaries are mutually compatible.

have different net displacements, no single image point represents the hangingwall in displacement space (Wojtal 1982, McCaig 1988). The chords which connect the images of different parts of the hangingwall indicate that the relative movements across fault bends, like the relative movements of portions of grains during grain boundary sliding (Brunner & Grant 1959), can be described as simple shear parallel to a particular plane. In the case of a concave fault bend, the shear plane bisects the bend. As Suppe (1983) noted, the attitudes of fold hinges (shear planes) at convex bends have more degrees of freedom. Geologically distinctive but kinematically equivalent deformation elements, such as kink bands, shear zones or subsidiary faults (Fig. 6), may appear in these settings, provided that the net offsets across those elements are compatible with the offsets on the faults.

Rocks with stylolites or veins

Considering only the construction of a displacement diagram, there are no reasons to limit *a priori* the movement of neighbouring blocks to displacements parallel to their common boundary or to rule out the formation of 'gaps' or 'overlaps' during deformation. Those restrictions exist in many settings, but the diagram itself can be used to analyze deformations where material is removed or added along block boundaries (e.g. by solution transfer). In those cases, a displacement diagram could be used to test if block displacements are mutually compatible by seeing if closed traverses in physical space produce closed loops in displacement space (Fig. 7).

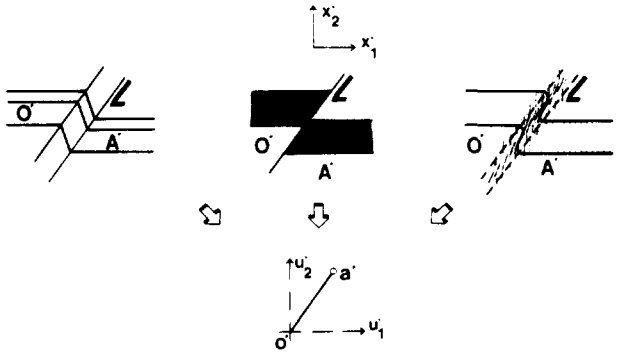

Fig. 6. Geologically distinct but kinematically equivalent deformation elements may have similar appearance in displacement space.

The method for measuring strains in faulted rocks outlined above can also be applied to volume-change deformations, i.e. rocks with stylolite or vein sets. Consider a section normal to a hypothetical array of stylolites where the displacements associated with the removal of mass along the stylolites (without local reprecipitation) conform with an imposed homogeneous deformation (Fig. 8a). Figure 8(b) is a displacement diagram constructed for lithons O', P', etc., encountered along two orthogonal traverses across the section. A plot of reciprocal displacement of lithons vs distance along each traverse (Fig. 8c) estimates the displacement gradients in this setting. Bulk strain values calculated from the measured displacement gradient values, illustrated by the Mohr diagram in Fig. 8(d), are good estimates of the principal directions, principal stretches, and area ratio of the imposed deformation.

Field example

Figure 9(a) is a downplunge projection, drawn on a principal plane, of a fault array in Pennsylvanian strata at the base of the Cumberland Plateau thrust sheet (Wojtal 1982, 1986, Wilson & Wojtal 1986). Since faults in the array, particularly low-angle reverse faults, are not planar, deformation could not have occurred solely by slip on faults. The heights of ramps in the reverse faults are small relative to offsets on the faults, so net displacements, measured relative to an origin at one end of a traverse across several fault-bounded blocks, of different portions of fault hangingwalls are nearly equal (Fig. 5). The intra-block deformation which occurs near ramps in low-angle faults does not introduce gross dis-

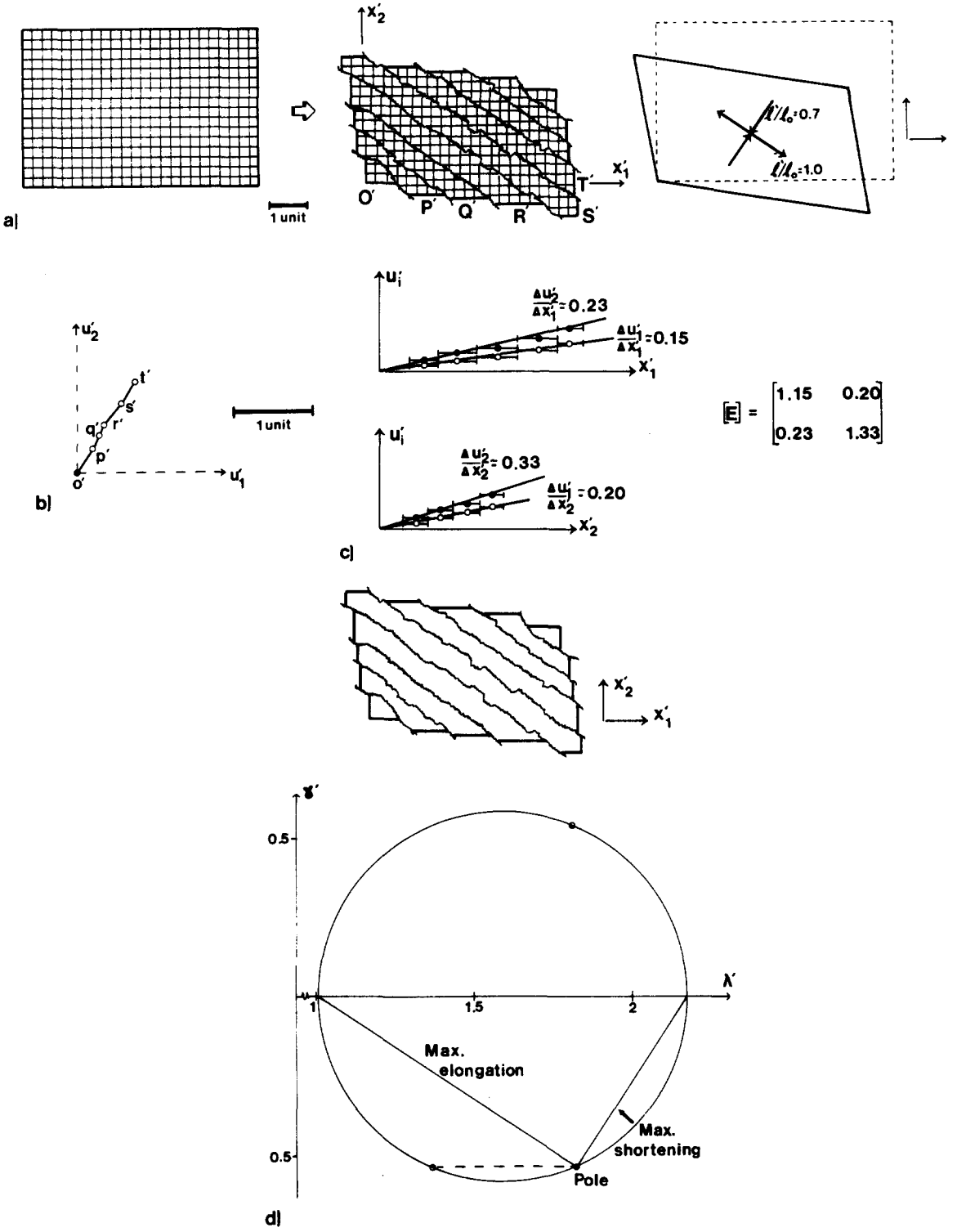

Fig. 8. (a) Hypothetical deformation by removing material along stylolite surfaces. The removal of material along the surfaces causes displacements of points in the grid which correspond to those in the homogeneous deformation depicted at right. (b) Diagram showing displacements of lithons crossed by traverses along the x'_1–x'_2 axes on (a). (c) Plots of components of the cumulative displacement (relative to an origin at the end of the traverse) of lithons (u'_i) vs distance along each traverse (x'_j). Open circles are u'_1 components and filled circles are u'_2 components. $\Delta u'_i/\Delta x'_j$ values are estimated from 'eyeball' fits to data. Components of matrix **E** calculated with equations (3). The area ratio of the imposed deformation = 0.70; the measured area ratio = 1/(det **E**) = 0.67. (d) Mohr diagram for reciprocal quadratic elongation, drawn using values calculated from displacement gradient values given in (c). The physical plane sketch above the Mohr diagram shows attitudes of the x'_1–x'_2 axes for plotted position of the pole to the Mohr circle. The measured orientations of the principal directions differ from the principal directions of the imposed deformation by 2°. The measured minimum stretch value is 0.68; the minimum stretch of the imposed deformation is 0.7. The measured maximum stretch value is 0.99; the maximum stretch of the imposed deformation is 1.0.

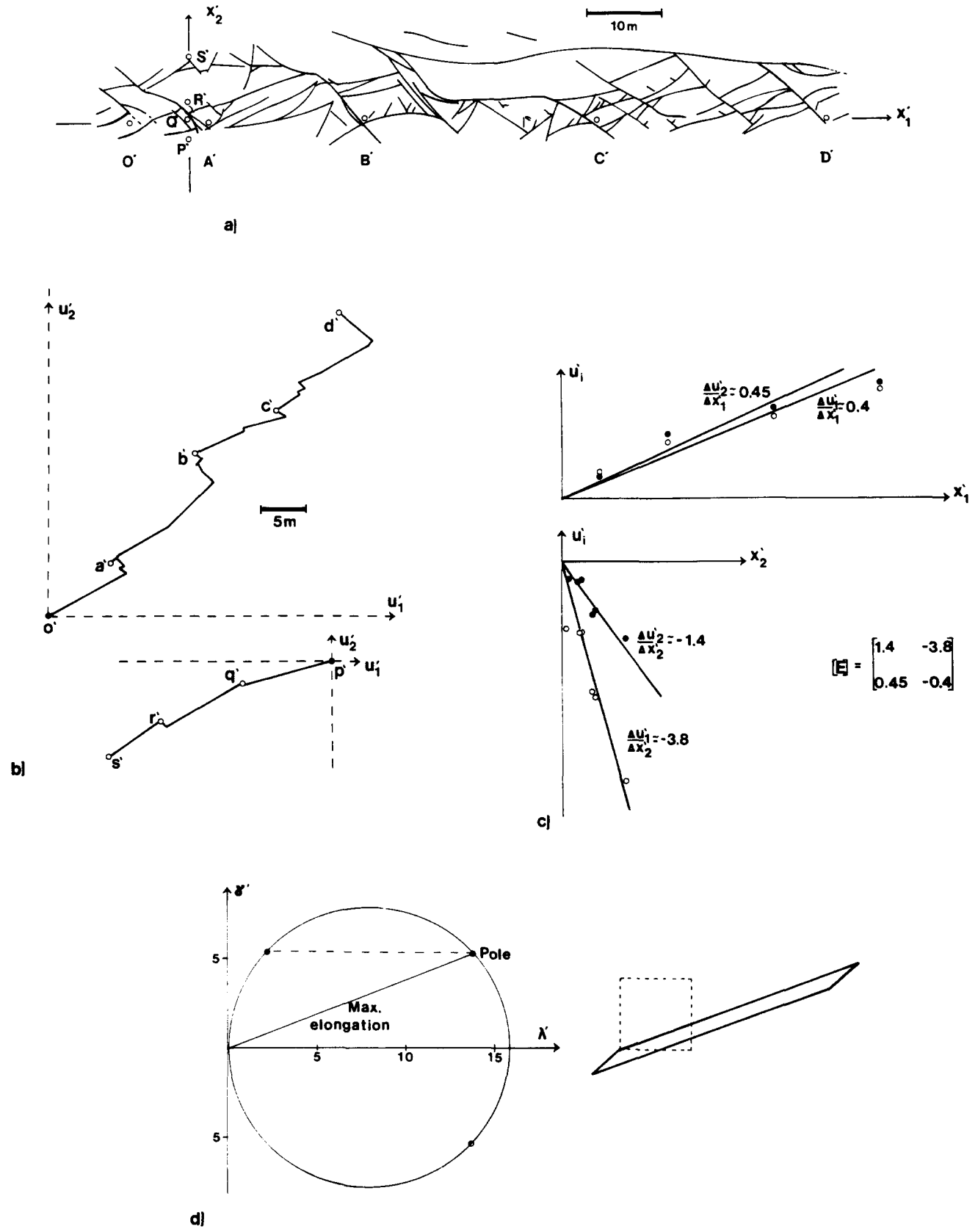

Fig. 9. (a) Section of pervasively faulted Pennsylvanian strata just above the Cumberland Plateau thrust fault, constructed by projecting structures onto a single plane inferred to be a principal plane of the deformation (see Wojtal 1982, 1986, Wilson & Wojtal 1986). x'_1 and x'_2 axes give the orientation of the traverses across the section. O', A', etc., are individual fault-bounded blocks. (b) Displacement diagram for fault-bounded blocks crossed along the two traverses across the section in (a). (c) Plot of displacement components u'_i vs position along co-ordinate axes x'_1 or x'_2. Open circles are u'_1 components; filled circles are u'_2 components. $\Delta u'_i/\Delta x'_j$ values are estimated from 'eyeball' fits to data. (d) Mohr diagram for reciprocal quadratic elongation drawn using strain values calculated from displacement gradient values derived in (c) with equations (5). Dashed square and solid parallelogram at right indicate the initial and final states corresponding to the measured strain values.

parities into the displacements of fault-bounded blocks measured in different traverses across a section. Figure 9(b) gives the displacements, derived from fault attitudes and offsets measured in the field and on Fig. 9(a), of material points which presently fall on two orthogonal traverses across Fig. 9(a). Plots of reciprocal displacement components u_i' vs position x_j' (Fig. 9c) estimate displacement gradients due to fault movement. A Mohr diagram for reciprocal quadratic elongations calculated from these displacement gradient values (Fig. 9d) gives the bulk strains due to movement on faults.

The strain values reported here are similar in outline but different in detail from those reported by Wojtal (1986), owing to the use of slopes of u_i' vs x_2' plots instead of intercepts of u_i' vs x_1' plots to calculate $\Delta u_i'/\Delta x_2'$ values. As noted above, the four-slope method yields better estimates of imposed strains in hypothetical situations. Furthermore, the area ratio in these rocks is larger (0.905) with the 'better' strain values. It is, then, easier to reconcile strain values in strata immediately adjacent to the thrust, where Wojtal (1986) reported small area ratios, with those in strata farther from the thrust, where area ratios are near unity. The strains still have the strong rotational component expected in a fault zone.

The measured strains are good estimates of the total deformation only in as far as the total deformation is statistically homogeneous. Inspection of the displacement vs position plots (Fig. 9c) shows that displacements are not strict linear functions of position, and underscores that strain values given here record only the 'first-order' change of shape due to movement on faults. Departure from homogeneity (non-linearity in displacement vs position plots) may be due to (1) errors in measuring fault offsets, (2) smooth curves or sharp bends in faults or (3) superposed inhomogeneous strains not associated with systematic deformation structures or microstructures (Cooper *et al.* 1983). All three effects are likely to contribute to non-linearity in displacement fields. Nevertheless, these 'first-order' strain values provide insight to the kinematics of the deformation due to movement on arrays of faults, and may aid in analyzing the mechanics of fault arrays. This is particularly true in cases where, like the Cumberland Plateau thrust zone, systematic grain-scale deformation structures are lacking.

SUMMARY

Deformation which is inhomogeneous, and possibly discontinuous, at one scale of observation may be statistically homogeneous when observed at a smaller scale. In statistically homogeneous deformations, where displacement gradient values are approximately constant, bulk strains can be defined. To measure strains within a principal plane of a discontinuous, but statistically homogeneous, deformation with constant area ratio:

(1) draw an accurate section of the deformed rocks;

(2) inscribe co-ordinate axes across the section with an arbitrary orientation;

(3) construct displacement diagrams for material points which presently fall on two mutually perpendicular axes, using offsets measured in the field or on the section through the deformed rocks;

(4) plot the components of the reciprocal displacement vectors for individual fault-bounded blocks along the traverse line against the positions of the fault-bounded blocks relative to the assigned origin. In homogeneous deformations, the reciprocal displacement vector component values fall along straight lines whose slopes are displacement gradient values;

(5) substitute the displacement gradient values into equation (5) (or its equivalent for the desired strain parameter) and calculate strain values.

Acknowledgements—I began working on the method outlined in this manuscript as a graduate student with David Elliott. His impact on this work was significant and is, I hope, apparent. I thank Oberlin College for releasing me from teaching responsibilities, and the Department of Geology and Geophysics at the University of Minnesota for providing me with a stimulating and comfortable setting to revise my earlier work. I also thank Joe Hull, Peter Hudleston, Christian Teyssier and the structural geology graduate students at Minnesota for critical yet encouraging comments on later versions of the work. Critical reviews by David Sanderson and an anonymous referee substantially improved the manuscript.

REFERENCES

Angelier, J. 1984. Tectonic analysis of fault slip data sets. *J. geophys. Res.* **89**, 5835–5848.

Arthaud, F. 1969. Méthode de détermination graphique des directions de raccourassement, d'allongement et intermediare d'une population des failles. *Bull. Soc. géol. Fr.*, 7 *Ser.* **11**, 729–737.

Arthaud, F. & Choukroune, P. 1972. Méthode d'analyse de la tectonique cassante à l'aide des microstructures dans les zones peu déformées. Exemple de la plateforme Nord-Aquitaine. *Revue Inst. Fr. Pétrole* **27**, 715–732.

Arthaud, F. & Mattauer, M. 1969. Exemples de stylolites d'origine tectonique dans le Languedoc, leurs relations avec la tectonique cassante. *Bull. Soc. géol. Fr.*, 7 *Ser.* **11**, 738–744.

Brunner, H. & Grant, N. J. 1959. Deformation resulting from grain boundary sliding. *Trans. metall. Soc. A.I.M.E.* **215**, 48–56.

Cobbold, P. R. 1977. Description and origin of banded deformation structures. I. Regional strain, local perturbations, and deformation in bands. *Can. J. Earth Sci.* **14**, 1721–1731.

Cooper, M. A., Garton, M. R. & Hossack, J. R. 1983. The origin of the Basse Normandie duplex, Boulonnais, France. *J. Struct. Geol.* **5**, 139–153.

Cox, A. & Hart, R. B. 1986. *Plate Tectonics: How it Works*. Blackwell Scientific, London.

Cutler, J. & Elliott, D. 1983. The compatibility equations and the pole to the Mohr circle. *J. Struct. Geol.* **5**, 287–297.

De Paor, D. 1979. The use of stereovectors in structural and engineering geology. *Tectonophysics* **60**, T1–T6.

De Paor, D. 1983. Orthographic analysis of geological structures—I. Deformation theory. *J. Struct. Geol.* **5**, 255–277.

Elliott, D. 1970. Determination of finite strain and initial shape from deformed elliptical objects. *Bull. geol. Soc. Am.* **81**, 2221–2236.

Etchecopar, A., Vasseur, G. & Daignieres, M. 1981. An inverse problem in microtectonics for the determination of stress tensors from fault striation analysis. *J. Struct. Geol.* **3**, 51–65.

Ford, H. 1963. *Advanced Mechanics of Materials*. Longmans, London.

Hancock, P. L. 1985. Brittle microtectonics principles and practice. *J. Struct. Geol.* **7**, 437–457.

Jamison, W. R. & Higgs, N. G. 1987. Fault/fracture strain: Wingate Sandstone. *Geol. Soc. Am. Abs. w. Prog.* **19**, 715.

King, G. 1983. The accommodation of large strains in the upper lithosphere of the earth and other solids by self-similar fault systems: the geometrical origin of *b*-value. *Pure & Appl. Geophys.* **121**, 761–815.

Kranz, R. W. 1988. Multiple fault sets and three-dimensional strain: theory and application. *J. Struct. Geol.* **10**, 225–238.

McCaig, A. 1988. Vector analysis of fault bends and intersecting faults. *J. Struct. Geol.* **10**, 121–124.

McKenzie, D. & Parker, R. 1967. The North Pacific: an example of tectonics on a sphere. *Nature* **216**, 1276–1280.

Paterson, M. S. & Weiss, L. E. 1961. Symmetry concepts in the structural analysis of deformed rocks. *Bull. geol. Soc. Am.* **72**, 841–882.

Philip, H. & Etchecopar, A. 1978. Exemple de variation de direction de cristallisation fibreuse dans un champ de constraintes unique. *Bull. Soc. géol., Fr.*, 7 *Ser.* **20**, 263–268.

Price, R. A. 1967. The tectonic significance of mesoscopic subfabrics in the southern Canadian Rocky mountains of Alberta and British Columbia. *Can. J. Earth Sci.* **4**, 39–70.

Ramsay, J. G. 1967. *Folding and Fracturing of Rocks*. McGraw-Hill, New York.

Ramsay, J. G. 1969. The measurement of strain and displacement in orogenic belts. In: *Time and Place in Orogeny* (edited by Kent, P. E., Satterthwaite, G. E. & Spenser, A. M.). *Spec. Publs geol. Soc. Lond.* **3**, 43–79.

Ramsay, J. G. 1976. Displacement and strain. *Phil. Trans. R. Soc. Lond.* **A283**, 3–25.

Ramsay, J. G. & Huber, M. 1983. *The Techniques of Modern Structural Geology. Volume* 1: *Strain Analysis*. Academic Press, London.

Rutter, E. 1986. On the nomenclature of mode of failure transitions. *Tectonophysics* **122**, 381–387.

Suppe, J. 1983. Geometry and kinematics of fault-bend folding. *Am. J. Sci.* **283**, 648–721.

Williams, G. D. & Chapman, T. 1983. Strains developed in the hangingwalls of thrusts due to their slip/propagation rate: a dislocation model. *J. Struct. Geol.* **5**, 563–571.

Wilson, R. L. & Wojtal, S. F. 1986. Cumberland Plateau décollement zone at Dunlap, Tennessee. In: *Centennial Field Guide* **6** (edited by Neathery, T. L.). *Geol. Soc. Am.*, Boulder, 143–148.

Wojtal, S. F. 1982. Finite deformation in thrust sheets and their material properties. Unpublished Ph.D. thesis, Johns Hopkins University, Baltimore, U.S.A.

Wojtal, S. 1986. Deformation within foreland thrust sheets by populations of minor faults. *J. Struct. Geol.* **8**, 426–435.

Wojtal, S. & Mitra, G. 1986. Strain hardening and strain softening in fault zones from foreland thrusts. *Bull. geol. Soc. Am.* **97**, 674–687.

Woodward, N. B., Gray, D. R. & Spears, D. B. 1986. Including strain data in balanced cross-sections. *J. Struct. Geol.* **8**, 313–324.